

# Engineering Favorable Propagation: Near-Field IRS Deployment for Spatial Multiplexing

Yuxuan Chen, Qingqing Wu, *Senior Member, IEEE*, Guangji Chen, Qiaoyan Peng, and Wen Chen, *Senior Member, IEEE*

**Abstract**—In intelligent reflecting surface (IRS)-assisted multiple-input multiple-output (MIMO) systems, a strong line-of-sight (LoS) link is required to compensate for the severe cascaded path loss. However, such a link renders the effective channel highly rank-deficient and fundamentally limits spatial multiplexing. To overcome this limitation, this paper leverages the large aperture of sparse arrays to harness near-field spherical wavefronts, and establishes a deterministic deployment criterion that strategically positions the IRS in the near-field of a base station (BS). This placement exploits the spherical wavefronts of the BS-IRS link to engineer decorrelated channels, thereby fundamentally overcoming the rank-deficiency issue in far-field cascaded channels. Based on a physical channel model for the sparse BS array and the IRS, we characterize the rank properties and inter-user correlation of the cascaded BS-IRS-user channel. We further derive a closed-form favorable propagation metric that reveals how the sparse array geometry and the IRS position can be tuned to reduce inter-user channel correlation. The resulting geometry-driven deployment rule provides a simple guideline for creating a favorable propagation environment with enhanced effective degrees of freedom. The favorable channel statistics induced by our deployment criterion enable a low-complexity maximum-ratio transmission (MRT) precoding scheme. This serves as the foundation for an efficient algorithm that jointly optimizes the IRS phase shifts and power allocation based solely on long-term statistical channel state information (CSI). Simulation results validate the effectiveness of our deployment criterion and demonstrate that our optimization framework achieves significant performance gains over benchmark schemes.

**Index Terms**—IRS, sparse MIMO, near-field communications, IRS deployment.

## I. INTRODUCTION

The pursuit of unprecedented spectral efficiency and ultra-high spatial resolution for sixth-generation (6G) systems has spurred the emergence of extremely large-scale multiple-input multiple-output (XL-MIMO) as a foundational technology [1]–[5]. By deploying antenna arrays with massive apertures, often operating at millimeter-wave or Terahertz frequencies, the communication environment inherently transitions from the conventional far-field to the more complex near-field region [6]. This near-field regime is characterized by a spherical electromagnetic wavefront, a fundamental shift that imbues the channel with a rich, distance-dependent spatial structure

Yuxuan Chen, Qingqing Wu, and Wen Chen are with the Department of Electronic Engineering, Shanghai Jiao Tong University, Shanghai 200240, China (e-mail: yuxuanchen@sjtu.edu.cn; qingqingwu@sjtu.edu.cn; wenchen@sjtu.edu.cn). Guangji Chen is with the School of Electronic and Optical Engineering, Nanjing University of Science and Technology, Nanjing 210094, China and also with National Mobile Communications Research Laboratory, Southeast University (email:guangjichen@njust.edu.cn). Qiaoyan Peng is with the State Key Laboratory of Internet of Things for Smart City, University of Macau, Macao 999078, China, and also with the Department of Electronic Engineering, Shanghai Jiao Tong University, Shanghai 200240, China (e-mail: qiaoyan.peng@connect.um.edu.mo).

[7]. The resulting additional spatial dimension allows for user separation based on not only angle but also range, creating new degrees of freedom (DoF) for communication [8]. Harnessing these near-field effects offers a new paradigm for enhancing spatial multiplexing and diversity, establishing near-field XL-MIMO as a key enabler for the ambitious performance targets of 6G [9].

However, realizing these benefits in practice is challenged by hardware constraints, cost, and power limitations. To address these challenges, sparse array architectures, where antenna elements are spaced wider than the traditional half-wavelength distance, have been introduced as an efficient means to expand the effective aperture without proportionally increasing hardware complexity [7]. Sparse uniform arrays (SUAs) can significantly enlarge the near-field region and enhance spatial focusing capability, making them particularly suitable for near-field communications. Recent near-field sparse array studies [10]–[13] further show that enlarging the effective array aperture via increased element spacing can extend the radiative near-field coverage and improve spatial resolution at essentially unchanged hardware cost. Nonetheless, the enlarged spacing substantially reshapes the array’s spatial response and maps users with distinct physical locations onto highly coupled effective channels, which leads to severe inter-user interference (IUI) [14]. Consequently, interference suppression in sparse MIMO systems remains a pressing research challenge, as conventional linear precoding and far-field-based designs, which rely on well-separated angular signatures, fail to cope with the spatial aliasing and channel correlation intrinsic to sparse geometries [15].

Intelligent reflecting surfaces (IRSs) have emerged as a transformative technology for reengineering the wireless propagation environment [16]–[21]. By controlling the phase shifts of a large number of low-cost passive elements, the IRS can manipulate signal reflections to constructively enhance desired links and destructively suppress interference [22]. A significant body of research has focused on exploiting this programmability for multiuser interference management in MIMO networks. To this end, the work [23] proposed a joint active and passive beamforming design to minimize interference leakage. Building upon these interference mitigation principles, the authors of [24] established a deterministic interference subspace alignment (ISA) framework which achieves the full multiplexing gain by completely eliminating interference. However, such methods often rely on instantaneous channel state information (CSI), which can impose prohibitive estimation overhead. The practical challenge of this overhead motivated subsequent research into designs based on slower-varying statistical CSI. In this domain, [25] demonstrated that

such approaches can optimize long-term performance metrics, such as ergodic sum-rate, with significantly reduced feedback, and [26] further analyzed the associated power scaling laws and phase shift optimization. Beyond algorithmic design, the physical deployment and topology of IRSs have also been exploited as effective DoF for suppressing inter-stream and inter-user interference [27]. Specifically, the authors in [28] proposed an orthogonal deployment of multiple IRSs, with spatially separated and oriented surfaces yielding orthogonal effective channels and mitigating mutual interference. Moreover, [29] showed that jointly optimizing the RIS deployment and reflection design can customize the composite channel rank and singular-value profile.

Despite these advances, a fundamental gap remains in understanding and designing IRS assisted sparse MIMO systems. Most existing IRS works assume purely far-field propagation, in which the base station (BS)-IRS channel collapses to a rank one structure, leading to fully correlated user channels and severely limiting multi-user multiplexing [30]. Recent near-field studies [31], [32] have started to model spherical wavefronts in XL-MIMO, revealing that wavefront curvature can significantly enhance DoF. Nevertheless, a critical open problem remains in translating this insight into practical design principles that can deterministically connect array sparsity and IRS placement with channel decorrelation. Furthermore, existing optimization frameworks typically depend on instantaneous CSI across the cascaded BS-IRS-user link, imposing prohibitive estimation overhead in large-scale deployments [25]. Thus, there is an urgent need for geometry-driven, deterministic, and statistically robust frameworks capable of harnessing near-field effects, sparse apertures, and intelligent reflection control to achieve scalable interference suppression and performance maximization.

In this paper, we develop a unified theoretical and algorithmic framework for sparse IRS assisted multiuser MIMO systems operating in a near-field regime. Building on a rigorous physical channel model, we jointly address the deterministic channel correlation, IRS deployment geometry, and statistical beamforming optimization. The key contributions are summarized as follows:

- First, we investigate the IRS-assisted multi-user communication system employing a hybrid sparse MIMO architecture, where a BS is equipped with a sparse uniform linear array (S-ULA) and the IRS is a sparse uniform planar array (S-UPA). To unveil the fundamental performance limits, we analyze the system from a spatial multiplexing perspective, utilizing the effective degree of freedom (EDoF) [33] as the evaluation metric. Specifically, we show that the enlarged apertures enabled by sparse arrays accentuate near-field spherical wavefronts on the BS-IRS link, thereby providing increased spatial resolution and improved user separability compared with the far-field regime. As a result, this sparse near-field configuration can achieve a substantially higher EDoF than conventional far-field IRS configuration in the LoS region of a BS.
- Next, we develop an analytical framework to characterize the rank properties of the cascaded BS-IRS-user channel.

In particular, we demonstrate that while far-field planar waves lead to rank-deficient channels, strategic IRS placement in the near-field of a BS leverages spherical wavefronts to create statistically independent sub-channels, thereby overcoming the inherent rank-deficiency of far-field cascaded channels. Based on this analysis, we derive a deterministic deployment criterion that provides a fundamental physical design principle for engineering channel statistics and enabling spatial multiplexing gain.

- Finally, we propose an efficient algorithm to maximize the ergodic sum-rate by leveraging statistical CSI. The BS adopts low-complexity maximum-ratio transmission (MRT) precoding, while an alternating optimization procedure is developed to jointly design the IRS phase shifts and user power allocation based solely on long-term channel statistics. Notably, we derive closed-form solutions for the subproblems within the iterative procedure. Numerical results demonstrate that, under the proposed deployment and algorithm, inter-user interference is effectively suppressed and the achieved EDoF and ergodic sum-rate are substantially improved over conventional IRS configurations, approaching the interference-free benchmark.

The remainder of the paper is organized as follows. Section II presents the system and channel models. Section III analyzes far- and near-field cascaded channels and derives the deployment criterion. Section IV proposes the statistical-CSI algorithm for ergodic sum-rate maximization. Section V provides numerical validations and performance evaluations. Section VI concludes the paper.

*Notations:* We use italic letters for scalars, boldface lower-case letters for vectors, and boldface upper-case letters for matrices. The operators  $\text{tr}(\cdot)$  and  $|\cdot|_F$  stand for the trace and Frobenius norm, respectively. The operator  $\text{diag}(\mathbf{a})$  returns a diagonal matrix with the elements of vector  $\mathbf{a}$  on its main diagonal. The statistical expectation and variance are denoted by  $\mathbb{E}[\cdot]$  and  $\text{var}\{\cdot\}$ . The function  $\text{gcd}(a, b)$  denotes the greatest common divisor of integers  $a$  and  $b$ . Finally,  $\mathcal{CN}(\boldsymbol{\mu}, \boldsymbol{\Sigma})$  denotes the circularly-symmetric complex Gaussian distribution with mean  $\boldsymbol{\mu}$  and covariance matrix  $\boldsymbol{\Sigma}$ .

## II. SYSTEM MODEL

As shown in Fig. 1, we consider a MIMO communication system, where a BS serves  $K$  users with the assistance of an IRS. The system is modeled in a three-dimensional Cartesian coordinate system, with the BS-IRS link characterized by a near-field channel model and the IRS-user links characterized by a far-field channel model. Furthermore, we assume that the direct BS-user links are obstructed due to practical blockage. The BS is equipped with an S-ULA comprising  $M$  antenna elements, where  $M$  is assumed to be an odd number for notational convenience. The array is aligned along the  $x$ -axis and centered at the origin. The position vector of the  $i$ -th antenna is given by  $\mathbf{p}_{\text{BS},i} = [id_{\text{BS}}, 0, 0]^T$ , where  $i \in \{0, \pm 1, \dots, \pm(M-1)/2\}$  and the inter-antenna spacing is defined as  $d_{\text{BS}} = \zeta_{\text{BS}} \frac{\lambda}{2}$  with  $\lambda$  denoting the carrier wavelength and  $\zeta_{\text{BS}}$  denoting the array sparsity factor at the BS. The IRS is an S-UPA comprising  $N = N_u \times N_v$  reflecting elements,

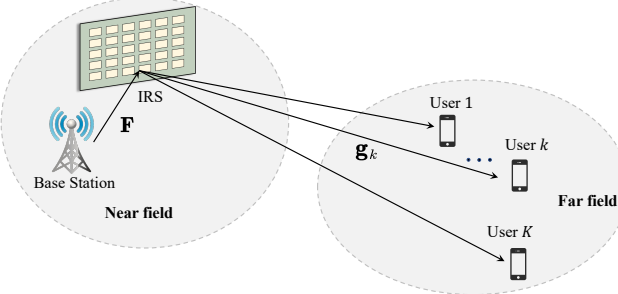


Fig. 1. IRS assisted multi-user sparse MIMO communication.

parallel to the  $y-z$  plane. The numbers of elements along the  $y$ - and  $z$ -axes,  $N_u$  and  $N_v$ , are both assumed to be odd. The geometric center of the IRS is located at  $\mathbf{r}_{\text{IRS}} = [l_x, l_y, l_z]^T$  with its distance from the origin being  $l = \|\mathbf{r}_{\text{IRS}}\|$ . The position vector of the  $(u_n, v_n)$ -th IRS element is  $\mathbf{p}_{\text{IRS},n} = \mathbf{r}_{\text{IRS}} + \boldsymbol{\delta}_n$ , where  $n \in \{1, 2, \dots, N\}$  and  $\boldsymbol{\delta}_n = [0, u_n d_{\text{IRS}}, v_n d_{\text{IRS}}]^T$  is the local displacement vector. Here, the pair  $(u_n, v_n)$  denotes the two-dimensional coordinates corresponding to the  $n$ -th element, with  $u_n = \lfloor \frac{n-1}{N_v} \rfloor - \frac{N_u-1}{2} \in \{0, \pm 1, \dots, \pm \frac{N_u-1}{2}\}$  and  $v_n = ((n-1) \bmod N_v) - \frac{N_v-1}{2} \in \{0, \pm 1, \dots, \pm \frac{N_v-1}{2}\}$ . The element spacing is defined as  $d_{\text{IRS}} = \zeta_{\text{IRS}} \lambda / 2$  with  $\zeta_{\text{IRS}}$  being the IRS sparsity factor. The channel between BS and IRS array is represented by  $\mathbf{F} \in \mathbb{C}^{M \times N}$  and the channel entry between the  $i$ -th BS antenna and the  $n$ -th IRS element is given by

$$[\mathbf{F}]_{i,n} = \rho_T e^{-j \frac{2\pi}{\lambda} d_{i,n}}, \quad (1)$$

where  $\rho_T$  is the complex-valued reference channel gain and  $d_{i,n} = \|\mathbf{p}_{\text{IRS},n} - \mathbf{p}_{\text{BS},i}\|$  denotes the distance between the  $i$ -th BS antenna to the  $n$ -th IRS element that can be further expressed as

$$d_{i,n} = \sqrt{(l_x - id_{\text{BS}})^2 + (l_y + u_n d_{\text{IRS}})^2 + (l_z + v_n d_{\text{IRS}})^2}. \quad (2)$$

Then, the far-field channel from the IRS to the  $k$ -th user  $\mathbf{g}_k \in \mathbb{C}^{N \times 1}$  can be expressed as

$$\mathbf{g}_k = \rho_{R,k} \mathbf{a}_{S,k} (\Phi_{R,k}^{\text{AOD}}, \Theta_{R,k}^{\text{AOD}}), \quad (3)$$

where  $\rho_{R,k}$  is the complex channel gain,  $\Phi_{R,k}^{\text{AOD}} = \pi \zeta_{\text{IRS}} \cos \theta_{R,k}^{\text{AOD}}$  and  $\Theta_{R,k}^{\text{AOD}} = \pi \zeta_{\text{IRS}} \sin \phi_{R,k}^{\text{AOD}} \sin \theta_{R,k}^{\text{AOD}}$  with  $\theta_{R,k}^{\text{AOD}}$  and  $\phi_{R,k}^{\text{AOD}}$  denoting the horizontal angle of departure (AoD) and the vertical AoD at the IRS, respectively. Furthermore, the array response vector  $\mathbf{a}_L$  of ULA can be unified by

$$\mathbf{a}_L (X) = [1, e^{jX}, \dots, e^{jX(L-1)}]^T. \quad (4)$$

It is worth noting that the array response  $\mathbf{a}_{S,k}$  for UPA can be decomposed into that of ULA as  $\mathbf{a}_{S,k} (X, Y) = \mathbf{a}_{N_u} (X) \otimes \mathbf{a}_{N_v} (Y)$ , where  $\otimes$  is the Kronecker product. Moreover, the passive beamforming matrix of the IRS is denoted by  $\boldsymbol{\Theta} = \text{diag}(e^{j\phi_1}, e^{j\phi_2}, \dots, e^{j\phi_N})$ . Thus, the cascaded channel from

the BS to the  $k$ -th user via the IRS is expressed as

$$\mathbf{h}_k = \mathbf{F} \boldsymbol{\Theta} \mathbf{g}_k. \quad (5)$$

Let  $\mathbf{W} = [\mathbf{w}_1, \mathbf{w}_2, \dots, \mathbf{w}_K] \in \mathbb{C}^{M \times K}$  denote the linear precoding matrix at the BS, where  $\mathbf{w}_k \in \mathbb{C}^{M \times 1}$  is the precoding vector for user  $k$ . The baseband transmitted signal is given by  $\mathbf{W}\mathbf{s}$ , where  $\mathbf{s} = [s_1, \dots, s_K]^T$  is the data vector with each element  $s_k$  being an independent variable with zero mean and normalized power. The received signal at user  $k$  can be expressed as

$$y_k = \mathbf{h}_k^H \mathbf{w}_k s_k + \sum_{j=1, j \neq k}^K \mathbf{h}_k^H \mathbf{w}_j s_j + \mathbf{z}_k, \quad (7)$$

where  $\mathbf{z}_k \sim \mathcal{CN}(0, \sigma_k^2)$  is the additive white Gaussian noise at user  $k$  with power  $\sigma_k^2$ . Accordingly, the signal-to-interference-plus-noise ratio (SINR) at the user  $k$  is given by

$$\gamma_k = \frac{|\mathbf{h}_k^H \mathbf{w}_k|^2}{\sum_{j=1, j \neq k}^K |\mathbf{h}_k^H \mathbf{w}_j|^2 + \sigma_k^2}. \quad (8)$$

Thus, the achievable sum rate of the system is given by

$$R = \sum_{k=1}^K R_k \triangleq \sum_{k=1}^K \log_2 (1 + \gamma_k). \quad (9)$$

### III. IRS DEPLOYMENT STRATEGY IN SPARSE MIMO

#### A. Channel Correlation Analysis in far-field

Consider the scenario where the IRS is located in the far-field of the BS, which requires the distance  $l$  to satisfy  $l > \frac{2(D_{\text{BS}} + D_{\text{IRS}})^2}{\lambda}$ , with  $D_{\text{BS}}$  and  $D_{\text{IRS}}$  denoting the apertures of the BS and IRS arrays, respectively [34]. Then, the spherical wavefronts emanating from the transmit antennas can be accurately approximated as planar waves at the receiver. The planar wave assumption is mathematically captured by a first-order Taylor series expansion of the propagation distance:

$$d_{i,n} \approx l - id_{\text{BS}}\mu_x + u_n d_{\text{IRS}}\mu_y + v_n d_{\text{IRS}}\mu_z, \quad (10)$$

where  $\mu_x = l_x/l$ ,  $\mu_y = l_y/l$ , and  $\mu_z = l_z/l$  are the direction cosines of the IRS's center relative to the BS.

Under this approximation, the channel matrix  $\mathbf{F}$  becomes rank-deficient, specifically rank-one. It can be expressed as

$$\mathbf{F} \approx \rho_T \mathbf{a}_M (\Theta_T^{\text{AOD}}) \mathbf{a}_S^H (\Phi_T^{\text{AOA}}, \Theta_T^{\text{AOA}}), \quad (11)$$

where  $\Theta_T^{\text{AOD}}$  and  $(\Phi_T^{\text{AOA}}, \Theta_T^{\text{AOA}})$  are determined by the AoD at the BS and the angles of arrival (AoA) at the IRS similarly in (3), respectively.

To quantify the impact of this rank-one channel  $\mathbf{F}$  on multi-user performance, we examine the spatial correlation between the cascaded channels of two arbitrary users,  $j$  and  $k$ , defined by the correlation coefficient:

$$\rho_{jk} = \frac{|\mathbf{h}_j^H \mathbf{h}_k|}{\|\mathbf{h}_j\| \|\mathbf{h}_k\|}. \quad (12)$$

With the IRS located in the far field of the BS, the cascaded channel for user  $k$  simplifies to  $\mathbf{h}_k \approx \chi_k \mathbf{a}_M (\Theta_T^{\text{AOD}})$ , where

$\chi_k = \rho_T \rho_{R,k} \mathbf{a}_S^H (\Phi_T^{\text{AOA}}, \Theta_T^{\text{AOA}}) \Theta \mathbf{a}_{S,k} (\Phi_{R,k}^{\text{AOD}}, \Theta_{R,k}^{\text{AOD}})$ . The correlation coefficient thus becomes:

$$\rho_{jk} \approx \frac{|\chi_j^* \chi_k \mathbf{a}_M^H (\Theta_T^{\text{AOD}}) \mathbf{a}_M (\Theta_T^{\text{AOD}})|}{|\chi_j \chi_k| M} = 1. \quad (13)$$

The result  $\rho_{jk} \approx 1$  indicates that the users' channels are perfectly correlated in the far-field LoS scenario. It implies that the users are spatially indistinguishable from the BS's perspective, rendering linear precoding ineffective for multi-user spatial multiplexing. This fundamental limitation severely degrades system performance.

### B. Near-Field Channel Modeling and Analysis

The fundamental limitation of the far-field model is that users' spatial signatures become perfectly correlated, which renders multi-user multiplexing ineffective. This motivates a transition to near-field analysis, where the spherical nature of the wavefront is explicitly taken into account. In this regime, which is characterized by the condition  $l < \frac{2(D_{\text{BS}}+D_{\text{IRS}})}{\lambda}$ , the path-length variations across the array elements are no longer linear.

To accurately capture this wavefront curvature, we employ a second-order Taylor series expansion for the distance  $d_{i,n}$  in (6):

$$\begin{aligned} d_{i,n} \approx l + \frac{\lambda}{2} & (-i\zeta_{\text{BS}}\mu_x + u_n\zeta_{\text{IRS}}\mu_y + v_n\zeta_{\text{IRS}}\mu_z) \\ & + \frac{\lambda^2}{8l} [(i\zeta_{\text{BS}})^2(1 - \mu_x^2) + (u_n\zeta_{\text{IRS}})^2(1 - \mu_y^2) + (v_n\zeta_{\text{IRS}})^2(1 - \mu_z^2)] \\ & + \frac{\lambda^2}{4l} (iu_n\zeta_{\text{BS}}\zeta_{\text{IRS}}\mu_x\mu_y + iv_n\zeta_{\text{BS}}\zeta_{\text{IRS}}\mu_x\mu_z - u_nv_n\zeta_{\text{IRS}}^2\mu_y\mu_z). \end{aligned} \quad (14)$$

To assess the attainable spatial multiplexing gain, we adopt the EDoF as a performance metric. For an aggregate multi-user channel matrix  $\mathbf{H} = [\mathbf{h}_1, \dots, \mathbf{h}_K]$ , the EDoF is defined as [33]

$$\varepsilon = \left( \frac{\text{tr}(\mathbf{H}\mathbf{H}^H)}{\|\mathbf{H}\mathbf{H}^H\|_F} \right)^2, \quad (15)$$

where an EDoF value approaching the number of users  $K$  signifies spatially orthogonal channels suitable for multiplexing. To assess the fundamental capabilities of the propagation environment, we evaluate the expected EDoF,  $E[\varepsilon]$ , by averaging over numerous realizations of i.i.d. random IRS phase shifts.

The impact of leveraging near-field effects through sparse arrays is illustrated in Fig. 2. The results demonstrate that array sparsity acts as a critical enabler for spatial multiplexing. Specifically, the conventional dense array configuration ( $\zeta_{\text{BS}} = 1, \zeta_{\text{IRS}} = 1$ ) yields an expected EDoF that remains close to 1, which reflects the rank-deficient nature of the channel in this regime. In contrast, increasing the sparsity factors substantially enhances the EDoF. This improvement

stems from the expanded effective apertures, which accentuate the wavefront curvature and generate distinct spatial signatures for users. Furthermore, this gain diminishes as the IRS-BS distance increases, confirming that the high degrees of freedom are intrinsically tied to the near-field propagation conditions.

To rigorously characterize this inherent capability, we analyze the channel's statistical properties under the assumption that the IRS phase shifts  $\{\phi_n\}$  are independent and identically distributed (i.i.d.) random variables drawn from a uniform distribution  $\mathcal{U}[0, 2\pi]$ . This approach allows us to characterize the fundamental propagation environment's sum-rate for user separation, abstracting away the specifics of any particular IRS beamforming configuration.

1) *Expected Inter-User Correlation*: To begin our analysis of the system's multi-user capabilities, we first evaluate the expected correlation between the channels of two distinct users,  $j$  and  $k$  as follows:

$$\mathbb{E}[\mathbf{h}_j^H \mathbf{h}_k] = \mathbf{g}_j^H \mathbb{E}[\Theta^H \mathbf{F}^H \mathbf{F} \Theta] \mathbf{g}_k. \quad (16)$$

Due to the statistical independence of the phase shifts, the expectation of the matrix product simplifies significantly. Specifically, for  $n \neq n'$ , the off-diagonal elements are zero since  $\mathbb{E}[e^{-j\phi_n} e^{j\phi_{n'}}] = \mathbb{E}[e^{-j\phi_n}] \mathbb{E}[e^{j\phi_{n'}}] = 0$ . The diagonal elements ( $n = n'$ ) evaluate to one, i.e.,  $\mathbb{E}[e^{-j\phi_n} e^{j\phi_n}] = 1$ . Consequently, the expected matrix becomes

$$\mathbb{E}[\Theta^H \mathbf{F}^H \mathbf{F} \Theta] = \text{diag}([\mathbf{F}^H \mathbf{F}]_{1,1}, \dots, [\mathbf{F}^H \mathbf{F}]_{N,N}). \quad (17)$$

Based on this, the expected inner product in (16) thus reduces to

$$\mathbb{E}[\mathbf{h}_j^H \mathbf{h}_k] = \sum_{n=1}^N [\mathbf{g}_j]_n^* [\mathbf{g}_k]_n \sum_{i=1}^M |\mathbf{F}_{i,n}|^2 = M |\rho_T|^2 (\mathbf{g}_j^H \mathbf{g}_k). \quad (18)$$

As the users are located in the far-field of the IRS,  $\mathbf{g}_j$  and  $\mathbf{g}_k$  are array response vectors corresponding to distinct spatial angles. For an IRS with a large aperture and sufficient angular separation between users, these vectors are nearly orthogonal. Consequently, the magnitude of their inner product  $|\mathbf{g}_j^H \mathbf{g}_k|$  is significantly suppressed, making the expected correlation  $\mathbb{E}[\mathbf{h}_j^H \mathbf{h}_k]$  negligible for  $j \neq k$ . This demonstrates that the user channels are, on average, weakly correlated, a foundational property for enabling multi-user communication.

2) *Favorable Propagation Analysis*: For robust multi-user communication, a powerful property is favorable propagation, which ensures that as the number of antennas grows the channel vectors of different users become deterministically orthogonal [35]. Favorable propagation is formally achieved if the normalized variance of the channel inner product vanishes:

$$g_{jk} \triangleq \frac{\text{var} \{ \mathbf{h}_j^H \mathbf{h}_k \}}{\mathbb{E} [\|\mathbf{h}_j\|^2] \mathbb{E} [\|\mathbf{h}_k\|^2]} \rightarrow 0, \quad \text{for } j \neq k. \quad (19)$$

The magnitude of  $g_{jk}$  quantifies the severity of inter-user interference (IUI), with a vanishing  $g_{jk}$  indicating asymptotic

$$\begin{aligned} d_{i,n} &= \sqrt{(l_x - id_{\text{BS}})^2 + (l_y + u_n d_{\text{IRS}})^2 + (l_z + v_n d_{\text{IRS}})^2} \\ &= l \sqrt{1 + \frac{\lambda}{l^2} (-il_x\zeta_{\text{BS}} + u_nl_y\zeta_{\text{IRS}} + v_nl_z\zeta_{\text{IRS}}) + \frac{\lambda^2}{4l^2} ((i\zeta_{\text{BS}})^2 + (u_n\zeta_{\text{IRS}})^2 + (v_n\zeta_{\text{IRS}})^2)} \end{aligned} \quad (6)$$

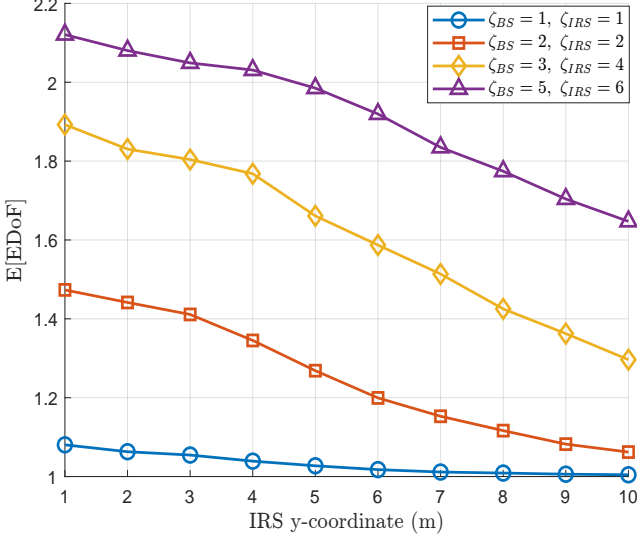


Fig. 2.  $\mathbb{E}[\text{EDoF}]$  versus sparsity and IRS position when  $N=1600$ .

orthogonality. Since the behavior of  $g_{jk}$  is governed by the variance term  $\text{var}\{\mathbf{h}_j^H \mathbf{h}_k\}$ , we derive its closed form in the following lemma by leveraging the random IRS phase shifts.

*Lemma 1:* Assuming independent and uniformly distributed random IRS phase shifts, the variance of the inner product between the cascaded channels of distinct users  $j$  and  $k$  is given by

$$\text{var}\{\mathbf{h}_j^H \mathbf{h}_k\} = \sum_{n_1=1}^N \sum_{\substack{n_2=1, \\ n_2 \neq n_1}}^N |[\mathbf{g}_j]_{n_1}|^2 |[\mathbf{g}_k]_{n_2}|^2 |[\mathbf{F}^H \mathbf{F}]_{n_1, n_2}|^2. \quad (20)$$

*Proof:* Please refer to Appendix A. ■

*Theorem 1:* Under the near-field spherical-wavefront model, the favorable propagation metric  $g_{jk}$  of the sparse MIMO system can be approximated as

$$g_{jk} \approx \frac{1}{M^2 N^2} \sum_{s=-(N_u-1)}^{N_u-1} \sum_{t=-(N_v-1)}^{N_v-1} w(s, t) f_M(\Delta_{s,t}), \quad (21)$$

where  $w(s, t) = (N_u - |s|)(N_v - |t|)$  and  $f_M(x) = \left(\frac{\sin(Mx/2)}{\sin(x/2)}\right)^2$  denotes the squared Dirichlet kernel of order  $M$ . The corresponding phase increment  $\Delta_{s,t}$  is given by

$$\Delta_{s,t} \triangleq s \left( \frac{\pi \lambda}{2l} \zeta_{\text{BS}} \zeta_{\text{IRS}} \mu_x \mu_y \right) + t \left( \frac{\pi \lambda}{2l} \zeta_{\text{BS}} \zeta_{\text{IRS}} \mu_x \mu_z \right). \quad (22)$$

*Proof:* From Lemma 1,  $g_{jk}$  is determined by the squared modulus of the Gram-matrix element:

$$|[\mathbf{F}^H \mathbf{F}]_{n_1, n_2}|^2 = |\rho_T|^4 \left| \sum_{i=-\frac{M-1}{2}}^{\frac{M-1}{2}} e^{-j \frac{2\pi}{\lambda} (d_{i, n_1} - d_{i, n_2})} \right|^2. \quad (23)$$

Substituting the second-order Taylor expansion of  $d_{i,n}$  in (14) into the phase and taking the difference  $d_{i,n_1} - d_{i,n_2}$ , the terms depending only on  $i$  cancel out, and the phase can be written as

$$\frac{2\pi}{\lambda} (d_{i, n_1} - d_{i, n_2}) \approx i \Delta_{n_1, n_2} + \Phi_{n_1, n_2}. \quad (24)$$

The coefficient  $\Delta_{n_1, n_2}$  follows from the cross-term in (14):

$$\Delta_{n_1, n_2} = \frac{\pi \lambda}{2l} \zeta_{\text{BS}} \zeta_{\text{IRS}} \mu_x [\mu_y (u_{n_1} - u_{n_2}) + \mu_z (v_{n_1} - v_{n_2})], \quad (25)$$

which reduces to  $\Delta_{s,t}$  as defined in the theorem by letting  $s = u_{n_1} - u_{n_2}$  and  $t = v_{n_1} - v_{n_2}$ . The term  $\Phi_{n_1, n_2}$  collects all terms independent of  $i$  from (14):

$$\Phi_{n_1, n_2} = \pi \zeta_{\text{IRS}} (\mu_y s + \mu_z t) + \frac{\pi \lambda}{4l} \zeta_{\text{IRS}}^2 [(u_{n_1}^2 - u_{n_2}^2)(1 - \mu_y^2) + (v_{n_1}^2 - v_{n_2}^2)(1 - \mu_z^2) - 2\mu_y \mu_z (u_{n_1} v_{n_1} - u_{n_2} v_{n_2})]. \quad (26)$$

Substituting this into the summation, the factor independent of  $i$  can be pulled out and disappears under the modulus:

$$\left| e^{-j \Phi_{n_1, n_2}} \sum_{i=-\frac{M-1}{2}}^{\frac{M-1}{2}} e^{-j i \Delta_{s,t}} \right|^2 = \left| \frac{\sin(M \Delta_{s,t}/2)}{\sin(\Delta_{s,t}/2)} \right|^2 = f_M(\Delta_{s,t}). \quad (27)$$

Finally, regrouping the sum over all IRS element pairs  $(n_1, n_2)$  by their relative spatial lags  $(s, t)$  yields the expression in the theorem with multiplicity weight  $w(s, t)$ . ■

Theorem 1 establishes a direct link between the statistical user correlation and the BS array factor under random phasing. Unlike the constant correlation observed in far-field LoS channels, the appearance of the Dirichlet kernel  $f_M(\cdot)$  implies that the random interference floor is structured and governed by the phase difference  $\Delta_{s,t}$ . This reveals that the inter-user interference is not an immutable environmental property, but a manageable variable determined by how the sparse array geometry samples the near-field wavefront.

### C. Design Principles for Channel Decorrelation

The metric  $g_{jk}$  in (21), governed by the Dirichlet kernel, captures the complex interplay between the system's physical parameters. To distill fundamental design principles from this expression, we first analyze its asymptotic behavior. This reveals the distinct and crucial roles of the BS and IRS scales in enabling multi-user spatial multiplexing, leading to our first key proposition.

*Proposition 1:* For a system with fixed BS antennas  $M$  and random IRS phase shifts,  $g_{jk} \rightarrow 0$  cannot be achieved by solely increasing the IRS size  $N$ . In the asymptotic limit  $N \rightarrow \infty$ , the metric converges to a non-zero floor determined by  $M$ :

$$\lim_{N \rightarrow \infty} g_{jk} = \mathcal{C}(M) > 0, \quad (28)$$

where  $\mathcal{C}(M)$  is a constant independent of  $N$ .

*Proof:* The behavior of  $g_{jk}$  is governed by the asymptotic scaling of its numerator and denominator. The denominator, representing the product of expected channel powers, scales quadratically with the IRS size, i.e., it is of order  $O(N^2)$ . For the numerator in (21), as  $N \rightarrow \infty$ , the discrete summation over the relative indices  $(s, t)$  can be approximated by a Riemann integral over the normalized aperture domain. Since the Dirichlet kernel  $f_M(\cdot)$  is non-negative and its main lobe energy is independent of  $N$ , the weighted summation also exhibits an asymptotic growth rate of  $O(N^2)$ . Consequently,

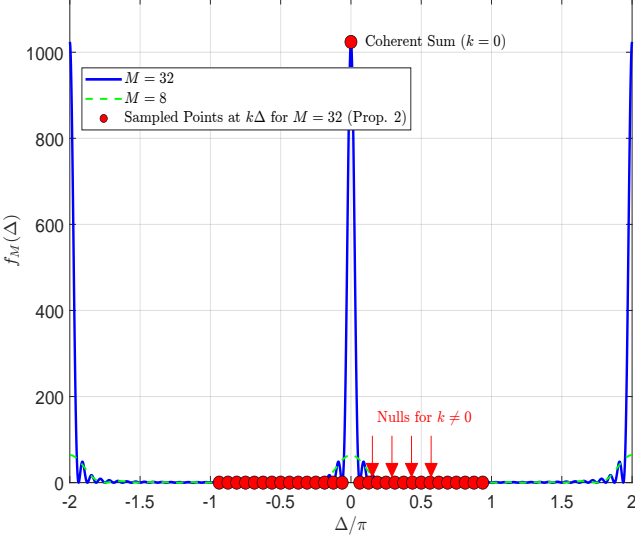


Fig. 3. Dirichlet kernel  $f_M(\Delta_{s,t})$  and sampled nulls.

the ratio defining  $g_{jk}$  converges to a strictly positive constant  $\mathcal{C}(M)$ . ■

Proposition 1 indicates that channel decorrelation is primarily enabled by a large BS aperture. This clarifies the distinct yet complementary roles of the BS and the IRS. The number of BS antennas  $M$  governs spatial separability, whereas the number of IRS elements  $N$  mainly contributes passive array gain to the link budget. This observation naturally leads to the question of whether we can move from merely exploiting favorable statistics to deterministically engineering decorrelated channels.

The structure of the Dirichlet kernel in (21) suggests that such deterministic engineering is indeed possible. As visualized in Fig. 3, the kernel exhibits a series of deep, periodic nulls. This deterministic structure presents an opportunity for proactive channel engineering: if the system geometry can be designed to place the inter-element phase differences  $\Delta_{s,t}$  precisely at these nulls, the cross-correlation terms in (21) can be systematically eliminated. Leveraging this ability to exploit the array factor's nulls through strategic geometric design, we establish the deployment criterion in the following proposition.

*Proposition 2:* Consider a symmetric IRS deployment satisfying  $\mu_y = \mu_z$ . Let the fundamental phase increment be defined as  $\Delta \triangleq \frac{\pi\lambda}{2\ell} \zeta_{\text{BS}} \zeta_{\text{IRS}} \mu_x \mu_y$ . If the system is designed such that

$$\Delta = \frac{q\pi}{M}, \quad (29)$$

where  $q$  is an even integer not a multiple of  $M$  and  $\gcd(\frac{q}{2}, M) = 1$  with  $M > N_u + N_v - 2$ . Thus, the metric  $g_{jk}$  simplifies to

$$g_{jk} = \frac{1}{(N_u N_v)^2} \sum_{s=-(N_{\min}-1)}^{N_{\min}-1} (N_u - |s|)(N_v - |s|), \quad (30)$$

where  $N_{\min} = \min(N_u, N_v)$ .

*Proof:* Under the symmetric deployment condition  $\mu_y = \mu_z$ , the two-dimensional phase dependency  $\Delta_{s,t}$  collapses to

a one-dimensional form,  $\Delta_{s,t} = (s+t)\Delta$ . By defining an auxiliary index  $k = s+t$ , the summation for  $g_{jk}$  can be regrouped as:

$$g_{jk} \propto \sum_{k=-(N_u+N_v-2)}^{N_u+N_v-2} W(k) f_M(k\Delta), \quad (31)$$

where  $W(k) = \sum_{s+t=k} (N_u - |s|)(N_v - |t|)$  is the aggregated weight for a given  $k$ . The condition  $\Delta = q\pi/M$  is specifically chosen to place the nulls of the Dirichlet kernel  $f_M(\cdot)$ . The kernel term  $f_M(k\Delta)$  is non-zero only when its argument  $k\Delta/2 = k(q\pi/M)/2$  is an integer multiple of  $\pi$ . This requires  $kq/M$  to be an even integer. Since  $q$  is not a multiple of  $M$ , this condition can only be met if  $k$  is a multiple of  $M$ .

The summation range for  $k$  is bounded by  $|k| \leq (N_u-1) + (N_v-1) = N_u + N_v - 2$ . The premise  $M > N_u + N_v - 2$  thus ensures that the only integer multiple of  $M$  within this range is  $k = 0$ . Consequently, all terms in the summation vanish except for the term corresponding to  $k = 0$ .

For  $k = 0$ , the kernel evaluates to its peak value,  $f_M(0) = M^2$ , and the condition  $k = s+t = 0$  implies  $s = -t$ . The expression for  $g_{jk}$  therefore simplifies to the contribution from this single term:

$$g_{jk} = \frac{1}{(N_u N_v)^2} \sum_{s=-(N_{\min}-1)}^{N_{\min}-1} (N_u - |s|)(N_v - |s|). \quad (32)$$

The summation is over all valid indices  $s$  such that  $t = -s$  is also a valid index. This constrains  $|s| \leq N_{\min} - 1$ , which completes the proof. ■

Proposition 2 captures the near-field geometric effect through the closed-form correlation term  $g_{jk}$  in (30). To obtain simple design rules with respect to the IRS size and the BS aperture, we next specialize to a square IRS with  $N_u = N_v = \sqrt{N}$ , which leads to the following corollary.

*Corollary 1:* Under the symmetric deployment conditions of Proposition 2, for an IRS with  $N_u = N_v = \sqrt{N}$ , the residual channel correlation metric  $g_{jk}$  is strictly upper-bounded by

$$g_{jk} < \frac{2}{M}. \quad (33)$$

*Proof:* When  $N_u = N_v = \sqrt{N}$ ,  $g_{jk}$  in (30) becomes  $g_{jk} = \frac{1}{N^2} \sum_{s=-(\sqrt{N}-1)}^{\sqrt{N}-1} (\sqrt{N} - |s|)^2$ . By applying the standard formula for the sum of squares, this summation evaluates to

$$g_{jk} = \frac{2N+1}{3N^{3/2}}. \quad (34)$$

Furthermore, we have

$$g_{jk} = \frac{2N+1}{3N^{3/2}} \stackrel{(a)}{<} \frac{1}{\sqrt{N}-1} \stackrel{(b)}{<} \frac{2}{M}, \quad (35)$$

where inequality (a) holds for all  $N \geq 1$  and inequality (b) is a direct result of the condition  $M > 2\sqrt{N} - 2$ . This completes the proof. ■

Proposition 2 and Corollary 1 reveal that a large-scale sparse MIMO system can be engineered to create a favorable transmission condition through judicious geometric design. By strategically selecting the IRS placement and array sparsities

to align inter-element phase differences with the nulls of the Dirichlet kernel, a high degree of channel decorrelation is achieved. This geometric approach provides a powerful mechanism to counteract the severe inter-user interference typically caused by sparse arrays, thereby rendering the channel substantially more favorable for spatial multiplexing. It thus alleviates the need for highly complex interference cancellation schemes at the transceiver and elevates deployment geometry to a powerful new degree of freedom for interference management.

#### IV. ERGODIC SUM-RATE MAXIMIZATION

##### A. Problem Formulation

While the preceding LoS analysis unveiled fundamental physical principles, practical wireless environments are characterized by multipath scattering. To model such scenarios, we now extend our framework by considering a Rician fading model for the IRS-user links, which adeptly captures both the deterministic LoS path and random non-line-of-sight (NLoS) components. The channel for user  $k$  is thus modeled as

$$\mathbf{g}_k = \sqrt{\frac{\alpha_k \kappa_k}{\kappa_k + 1}} \bar{\mathbf{g}}_k + \sqrt{\frac{\alpha_k}{\kappa_k + 1}} \tilde{\mathbf{g}}_k \quad (36)$$

$$= \sqrt{\alpha_k \beta_k} \bar{\mathbf{g}}_k + \sqrt{\alpha_k (1 - \beta_k)} \tilde{\mathbf{g}}_k, \quad (37)$$

where  $\alpha_k$  is the large-scale path gain,  $\beta_k = \frac{\kappa_k}{\kappa_k + 1}$ ,  $\kappa_k$  is the Rician factor,  $\bar{\mathbf{g}}_k$  is the deterministic LoS component, and  $\tilde{\mathbf{g}}_k \sim \mathcal{CN}(\mathbf{0}, \mathbf{I}_N)$  represents the normalized NLoS fading.

The favorable channel statistics designed by our deployment strategy, which significantly reduce inter-user channel correlation, motivate the adoption of a low-complexity precoding scheme. While precoders like Zero-Forcing (ZF) can eliminate interference, they entail high computational complexity due to matrix inversions, particularly in large-scale systems. Consequently, with inter-user interference already substantially suppressed by our near-field deployment, we employ MRT to maximize the desired signal power with reduced complexity. The precoding vector at the BS for user  $k$  under the MRT scheme is  $\mathbf{w}_k = \sqrt{p_k} \mathbf{h}_k$ , where  $p_k$  is the power allocation factor for user  $k$ . Furthermore,  $p_k$  is optimized under the total average transmit power constraint  $\sum_{k=1}^K p_k \mathbb{E}[\|\mathbf{h}_k\|^2] \leq P_{\max}$ , where the average is taken over the Rician fading statistics [36]. Our objective is to maximize the long-term system performance, which is characterized by the ergodic sum-rate as follows:

$$R_{\text{erg}} = \sum_{k=1}^K \mathbb{E}_{\{\bar{\mathbf{g}}_k\}} [\log_2(1 + \gamma_k)]. \quad (38)$$

However, directly optimizing (38) is difficult and a widely adopted and effective method to handle it is to optimize an approximation of the ergodic sum-rate based on statistical CSI. This leads to an effective SINR expression for user  $k$ :

$$\gamma_k^{\text{approx}} \triangleq \frac{p_k \mathbb{E}[\mathbf{h}_k^H \mathbf{h}_k]^2}{\sum_{j \neq k} p_j \mathbb{E}[\|\mathbf{h}_k^H \mathbf{h}_j\|^2] + \sigma_k^2}, \quad (39)$$

where

$$\mathbb{E}[\mathbf{h}_k^H \mathbf{h}_k] = C_k + \alpha_k \beta_k \boldsymbol{\theta}^H \mathbf{A}_{k,k} \boldsymbol{\theta}, \quad (40)$$

$$\begin{aligned} \mathbb{E}[\|\mathbf{h}_k^H \mathbf{h}_j\|^2] &= \alpha_k \alpha_j \beta_k \beta_j |\boldsymbol{\theta}^H \mathbf{A}_{k,j} \boldsymbol{\theta}|^2 + \alpha_k \alpha_j \beta_k (1 - \beta_j) \boldsymbol{\theta}^H \mathbf{D}_k \boldsymbol{\theta} \\ &\quad + \alpha_k \alpha_j \beta_j (1 - \beta_k) \boldsymbol{\theta}^H \mathbf{D}_j \boldsymbol{\theta} + C_{k,j} \end{aligned} \quad (41)$$

with  $C_k = \alpha_k (1 - \beta_k) \|\mathbf{F}\|_F^2$ ,  $C_{k,j} = \alpha_k \alpha_j (1 - \beta_k) (1 - \beta_j) \text{tr}((\mathbf{F} \mathbf{F}^H)^2)$ ,  $\mathbf{A}_{k,j} = \text{diag}(\bar{\mathbf{g}}_k)^H \mathbf{F}^H \mathbf{F} \text{diag}(\bar{\mathbf{g}}_j)$ ,  $\mathbf{D}_k = \text{diag}(\bar{\mathbf{g}}_k)^H \mathbf{F}^H \mathbf{F} \mathbf{F}^H \mathbf{F} \text{diag}(\bar{\mathbf{g}}_k)$ ,  $k, j \in \{1, 2, \dots, K\}$  and  $\boldsymbol{\theta} = [e^{j\phi_1}, e^{j\phi_2}, \dots, e^{j\phi_N}]^T$ . Please refer to Appendix B for more details.

Consequently, our optimization problem transforms into maximizing the approximate ergodic sum-rate by jointly designing the IRS phase shifts and the power allocation. The problem is thus formulated as

$$\max_{\boldsymbol{\theta}, \mathbf{p}} \quad \sum_{k=1}^K \log_2 (1 + \gamma_k^{\text{approx}}) \quad (42)$$

$$\text{s.t.} \quad |[\boldsymbol{\theta}]_n| = 1, \forall n \in \{1, \dots, N\}, \quad (42a)$$

$$\sum_{k=1}^K p_k \mathbb{E}[\|\mathbf{h}_k\|^2] \leq P_{\max}, p_k \geq 0, \forall k, \quad (42b)$$

where  $\mathbf{p} = [p_1, \dots, p_K]^T$ .

Since problem (42) is highly non-convex, to overcome it, we first reformulate the objective function into a more tractable form using a sequence of transformations, which enables an efficient alternating optimization algorithm. First, using the Lagrangian dual method, we introduce auxiliary variables  $\boldsymbol{\xi} = [\xi_1, \dots, \xi_K]^T$  [37]. The problem is equivalent to maximizing

$$\mathcal{L}_1(\boldsymbol{\theta}, \mathbf{p}, \boldsymbol{\xi}) = \sum_{k=1}^K \left[ \log_2(1 + \xi_k) - \xi_k + \frac{(1 + \xi_k) S_k(\boldsymbol{\theta}, p_k)}{J_k(\boldsymbol{\theta}, \mathbf{p}) + S_k(\boldsymbol{\theta}, p_k)} \right], \quad (43)$$

where  $S_k(\boldsymbol{\theta}, p_k) = p_k \mathbb{E}[\|\mathbf{h}_k^H \mathbf{h}_k\|^2]$  represents the statistical signal power and  $J_k(\boldsymbol{\theta}, \mathbf{p}) = \sum_{j \neq k} p_j \mathbb{E}[\|\mathbf{h}_k^H \mathbf{h}_j\|^2] + \sigma_k^2$  represents the statistical interference-plus-noise power. For fixed  $(\boldsymbol{\theta}, \mathbf{p})$ , the closed-form solution for (43) is

$$\xi_k^* = \frac{S_k(\boldsymbol{\theta}, p_k)}{J_k(\boldsymbol{\theta}, \mathbf{p})}, k = 1, \dots, K. \quad (44)$$

Next, we apply the quadratic transform with a second set of auxiliary variables  $\boldsymbol{\eta} = [\eta_1, \dots, \eta_K]^T$  [38]. This results in the objective:

$$\mathcal{L}_2(\boldsymbol{\theta}, \mathbf{p}, \boldsymbol{\xi}, \boldsymbol{\eta}) = \sum_{k=1}^K \left[ 2\eta_k \sqrt{(1 + \xi_k) S_k(\boldsymbol{\theta}, p_k)} - \eta_k^2 (J_k(\boldsymbol{\theta}, \mathbf{p}) + S_k(\boldsymbol{\theta}, p_k)) \right]. \quad (45)$$

For fixed  $(\boldsymbol{\theta}, \mathbf{p}, \boldsymbol{\xi})$ , the closed-form solution is

$$\eta_k^* = \frac{\sqrt{(1 + \xi_k) S_k(\boldsymbol{\theta}, p_k)}}{S_k(\boldsymbol{\theta}, p_k) + J_k(\boldsymbol{\theta}, \mathbf{p})}, k = 1, \dots, K. \quad (46)$$

The algorithm proceeds by iteratively updating  $(\boldsymbol{\xi}, \boldsymbol{\eta})$ ,  $\mathbf{p}$ , and  $\boldsymbol{\theta}$ .

##### B. Power Allocation Optimization

With the IRS phases  $\boldsymbol{\theta}$  and auxiliary variables  $(\boldsymbol{\xi}, \boldsymbol{\eta})$  held fixed, the subproblem for optimizing the power allocation

vector  $\mathbf{p}$  is derived from maximizing  $\mathcal{L}_2$ . Isolating the terms dependent on  $p_k$  for a single user, the objective for each  $p_k$  becomes

$$\begin{aligned} \max_{p_k} \quad & -c_{1,k}p_k + c_{2,k}\sqrt{p_k} \\ \text{s.t.} \quad & (42b). \end{aligned} \quad (47)$$

where  $c_{1,k} = \eta_k^2 \mathbb{E}[\|\mathbf{h}_k^H \mathbf{h}_k\|^2] + \sum_{j \neq k} \eta_j^2 \mathbb{E}[\|\mathbf{h}_j^H \mathbf{h}_k\|^2]$  and  $c_{2,k} = 2\eta_k \sqrt{1 + \xi_k} \mathbb{E}[\|\mathbf{h}_k^H \mathbf{h}_k\|]$ . Problem (47) is convex for each  $p_k$ . Thus, we can solve for the entire vector  $\mathbf{p}$  using a block coordinate descent (BCD) approach, where each  $p_k$  is updated iteratively. The optimal solution for a single  $p_k$ , given the others, has a closed-form as follows:

$$p_k^* = \min \left\{ \frac{P_{\max} - \sum_{j \neq k} p_j \mathbb{E}[\|\mathbf{h}_j\|^2]}{\mathbb{E}[\|\mathbf{h}_k\|^2]}, \left( \frac{c_{2,k}}{2c_{1,k}} \right)^2 \right\}. \quad (48)$$

### C. IRS Phase Shift Optimization

With the power allocation  $\mathbf{p}$  and auxiliary variables  $(\xi, \eta)$  fixed, the remaining subproblem is to optimize the IRS phase vector  $\boldsymbol{\theta}$ . Based on the surrogate function  $\mathcal{L}_2$ , it is equivalent to the following minimization problem:

$$\begin{aligned} \min_{\boldsymbol{\theta}} \quad & \boldsymbol{\theta}^H \mathbf{Q} \boldsymbol{\theta} + \sum_{k=1}^K \sum_{j=1}^K p_j \eta_k^2 \alpha_k \alpha_j \beta_k \beta_j |\boldsymbol{\theta}^H \mathbf{A}_{k,j} \boldsymbol{\theta}|^2 \\ \text{s.t.} \quad & |[\boldsymbol{\theta}]_n| \leq 1, \forall n \in \{1, \dots, N\}, \end{aligned} \quad (49)$$

$$(42b), \quad (49a)$$

where the complex matrix  $\mathbf{Q}$  is defined as

$$\begin{aligned} \mathbf{Q} = & - \left[ \sum_{k=1}^K \left( 2\eta_k \alpha_k \beta_k \sqrt{(1 + \xi_k)p_k} - 2\eta_k^2 p_k \alpha_k C_k \beta_k \right) \mathbf{A}_{k,k} \right] \\ & + \sum_{k=1}^K \eta_k^2 \sum_{j \neq k} p_j \alpha_k \alpha_j (\beta_k(1 - \beta_j) \mathbf{D}_k + \beta_j(1 - \beta_k) \mathbf{D}_j). \end{aligned} \quad (50)$$

To address the non-convexity of the unit-modulus constraint in (42a), we first relax it to the convex inequality in (49a) for tractable optimization, and then project the converged solution back via the mapping  $\theta_n \leftarrow e^{j \arg\{\theta_n\}}$ . However, problem (49) is still highly non-convex. We solve it using the Alternating Direction Method of Multipliers (ADMM) by introducing auxiliary variables  $\mathbf{z}, \mathbf{k}, \mathbf{s}$  and the consensus constraints  $\mathbf{z} = \boldsymbol{\theta}, \mathbf{k} = \boldsymbol{\theta}, \mathbf{s} = \boldsymbol{\theta}$ . The augmented Lagrangian is formulated as

$$\min_{\boldsymbol{\theta}, \mathbf{z}, \mathbf{k}, \mathbf{s}} \mathcal{L}_\rho(\boldsymbol{\theta}, \mathbf{z}, \mathbf{k}, \mathbf{s}) \quad (51)$$

$$\text{s.t.} \quad \mathbf{z} = \boldsymbol{\theta}, \mathbf{k} = \boldsymbol{\theta}, \mathbf{s} = \boldsymbol{\theta}, \quad (51a)$$

$$|[\mathbf{k}]_n| \leq 1, \forall n, \quad (51b)$$

$$\sum_{k=1}^K p_k \left( C_k + \alpha_k \beta_k \boldsymbol{\theta}^H \mathbf{A}_{k,k} \mathbf{s} \right) \leq P_{\max}, \quad (51c)$$

where  $\mathcal{L}_\rho(\boldsymbol{\theta}, \mathbf{z}, \mathbf{k}, \mathbf{s}) = \Re\{\boldsymbol{\theta}^H \mathbf{Q} \mathbf{z}\} + \rho \|\mathbf{z} - \boldsymbol{\theta} + \boldsymbol{\lambda}_z\|_2^2 + \sum_{k,j} p_j \eta_k^2 \alpha_k \alpha_j \beta_k \beta_j |\boldsymbol{\theta}^H \mathbf{A}_{k,j} \mathbf{z}|^2 + \rho \|\mathbf{k} - \boldsymbol{\theta} + \boldsymbol{\lambda}_k\|_2^2 + \rho \|\mathbf{s} - \boldsymbol{\theta} + \boldsymbol{\lambda}_s\|_2^2$ ,  $\rho > 0$  is the penalty parameter, and  $\boldsymbol{\lambda}_z, \boldsymbol{\lambda}_k, \boldsymbol{\lambda}_s$  are the scaled dual variables. The variables are updated iteratively:

### Algorithm 1 Proposed Algorithm for Problem(42)

- 1: **Initialize:** Set iteration counter  $t = 0$ , tolerance  $\epsilon$ . Initialize variables  $\mathbf{p}^{(0)}, \boldsymbol{\theta}^{(0)}, \mathbf{z}^{(0)}, \mathbf{k}^{(0)}, \mathbf{s}^{(0)}$  and dual variables  $\boldsymbol{\lambda}_z^{(0)}, \boldsymbol{\lambda}_k^{(0)}, \boldsymbol{\lambda}_s^{(0)}$  to feasible values.
- 2: **repeat**
- 3: Update auxiliary variables  $\boldsymbol{\xi}^{(t+1)}$  and  $\boldsymbol{\eta}^{(t+1)}$  by (44) and (46).
- 4: Update power allocation  $\mathbf{p}^{(t+1)}$  by (48).
- 5: Update primal variables  $\boldsymbol{\theta}^{(t+1)}, \mathbf{z}^{(t+1)}, \mathbf{k}^{(t+1)}, \mathbf{s}^{(t+1)}$  by (54), (57), (59), and (60), respectively.
- 6: Update dual variables  $\boldsymbol{\lambda}_z^{(t+1)}, \boldsymbol{\lambda}_k^{(t+1)}, \boldsymbol{\lambda}_s^{(t+1)}$  by (61).
- 7: Set  $t = t + 1$ .
- 8: **until** the improvement of the objective value of (42) is below  $\epsilon$ .
- 9: **Output:** The optimized power allocation  $\mathbf{p}^* = \mathbf{p}^{(t)}$  and phase shifts  $\theta_n \leftarrow e^{j \arg\{\theta_n\}}$ .

1) *Update for  $\boldsymbol{\theta}$ :* With  $(\mathbf{z}, \mathbf{k}, \mathbf{s})$  fixed, the subproblem for  $\boldsymbol{\theta}$  is an unconstrained quadratic minimization:

$$\min_{\boldsymbol{\theta}} \boldsymbol{\theta}^H (\mathbf{Y}(\mathbf{z}) + 3\rho \mathbf{I}) \boldsymbol{\theta} - 2\Re\{\boldsymbol{\theta}^H \mathbf{v}_\theta\} \quad (52)$$

where  $\mathbf{Y}(\mathbf{z}) = \sum_{k,j} \eta_k^2 p_j \alpha_k \alpha_j \beta_k \beta_j (\mathbf{A}_{k,j} \mathbf{z}) (\mathbf{z}^H \mathbf{A}_{k,j}^H)$  and we define the composite vector  $\mathbf{v}_\theta$  for notational simplicity:

$$\mathbf{v}_\theta \triangleq \rho(\mathbf{z} + \boldsymbol{\lambda}_z + \mathbf{k} + \boldsymbol{\lambda}_k + \mathbf{s} + \boldsymbol{\lambda}_s) - \frac{1}{2} \mathbf{Q} \mathbf{z}. \quad (53)$$

The closed-form solution is found by setting the gradient to zero:

$$\boldsymbol{\theta}^* = (\mathbf{Y}(\mathbf{z}) + 3\rho \mathbf{I})^{-1} \mathbf{v}_\theta. \quad (54)$$

2) *Update for  $\mathbf{z}$ :* Similarly, with other variables fixed, the subproblem for  $\mathbf{z}$  is:

$$\min_{\mathbf{z}} \mathbf{z}^H (\mathbf{Y}'(\boldsymbol{\theta}) + \rho \mathbf{I}) \mathbf{z} - 2\Re\{\mathbf{z}^H \mathbf{v}_z\} \quad (55)$$

where  $\mathbf{Y}'(\boldsymbol{\theta}) = \sum_{k,j} \eta_k^2 p_j \alpha_k \alpha_j \beta_k \beta_j (\mathbf{A}_{k,j}^H \boldsymbol{\theta}) (\boldsymbol{\theta}^H \mathbf{A}_{k,j})$  and the composite vector  $\mathbf{v}_z$  is

$$\mathbf{v}_z \triangleq \rho(\boldsymbol{\theta} - \boldsymbol{\lambda}_z) - \frac{1}{2} \mathbf{Q}^H \boldsymbol{\theta}. \quad (56)$$

The closed-form solution is

$$\mathbf{z}^* = (\mathbf{Y}'(\boldsymbol{\theta}) + \rho \mathbf{I})^{-1} \mathbf{v}_z. \quad (57)$$

3) *Update for  $\mathbf{k}$ :* The subproblem for  $\mathbf{k}$  is a projection onto the unit-modulus manifold:

$$\begin{aligned} \min_{\mathbf{k}} \quad & \|\mathbf{k} - (\boldsymbol{\theta} - \boldsymbol{\lambda}_k)\|_2^2 \\ \text{s.t.} \quad & (51b). \end{aligned} \quad (58)$$

The optimal update for each element of  $\mathbf{k}$  is given in the following closed form:

$$[\mathbf{k}^*]_n = \begin{cases} [\boldsymbol{\theta} - \boldsymbol{\lambda}_k]_n, & \text{if } |[\boldsymbol{\theta} - \boldsymbol{\lambda}_k]_n| \leq 1, \\ \frac{[\boldsymbol{\theta} - \boldsymbol{\lambda}_k]_n}{\|[\boldsymbol{\theta} - \boldsymbol{\lambda}_k]_n\|_2}, & \text{otherwise.} \end{cases} \quad (59)$$

4) *Update for  $\mathbf{s}$ :* The subproblem for  $\mathbf{s}$  is the convex quadratically constrained quadratic program (QCQP):

$$\begin{aligned} \min_{\mathbf{s}} \quad & \|\mathbf{s} - (\boldsymbol{\theta} - \boldsymbol{\lambda}_s)\|^2 \\ \text{s.t.} \quad & (51c). \end{aligned} \quad (60)$$

It can be solved efficiently using standard convex optimization solvers (CVX) [39].

5) *Dual Variable Updates:* The dual variables are updated via standard gradient ascent steps as follows:

$$\begin{cases} \boldsymbol{\lambda}_z^{t+1} = \boldsymbol{\lambda}_z^t + \mathbf{z} - \boldsymbol{\theta} \\ \boldsymbol{\lambda}_k^{t+1} = \boldsymbol{\lambda}_k^t + \mathbf{k} - \boldsymbol{\theta} \\ \boldsymbol{\lambda}_s^{t+1} = \boldsymbol{\lambda}_s^t + \mathbf{s} - \boldsymbol{\theta} \end{cases} \quad (61)$$

where  $t$  represents the iteration count.

The overall algorithm for (42) is summarized in Algorithm 1. The alternating optimization structure guarantees the algorithm's convergence to a stationary point. A key advantage of our framework is its reliance on a tractable analytical expression for the ergodic rate, which operates on long-term statistical CSI. This design obviates the need for frequent updates within each coherence interval, thereby substantially reducing feedback overhead. The total computational complexity of the algorithm is  $\mathcal{O}(I(K^2N^2 + N^{3.5}))$ , where  $I$  is the number of alternating optimization iterations required for convergence. The complexity ensures the algorithm's practicality in large-scale system deployments.

## V. NUMERICAL RESULTS

In this section, we provide numerical results to validate our theoretical analyses and demonstrate the performance of the proposed optimization algorithm. Unless specified otherwise, we consider a system with a carrier frequency of  $f = 60$  GHz. The BS is equipped with an S-ULA of  $M = 128$  antennas. The array sparsity factors are set to  $\zeta_{\text{BS}} = 3, \zeta_{\text{IRS}} = 6$ . Unless otherwise specified, the IRS is centered at  $\mathbf{r}_{\text{IRS}} = [-0.72m, 0.51m, 0.51m]^T$  with the location strategically chosen to create a favorable propagation environment that aligns with the principles derived in Proposition 2. We consider  $K = 4$  single-antenna users located at  $[10m, 70m, 0m]^T, [30m, 60m, 0m]^T, [20m, 50m, 0m]^T$ , and  $[45m, 45m, 0m]^T$ , respectively. The noise power is set to  $\sigma_k^2 = -115$  dBm for all users.

Fig. 4 illustrates the favorable propagation metric  $g_{jk}$  versus the IRS's y-coordinate for various array sparsity configurations when  $N = 1600$  and the IRS is centered at  $[-3m, l_y, 3m]$ . The analytical model from (21) shows excellent agreement with the Monte Carlo simulations, which confirms the fidelity of our near-field channel correlation model. It also demonstrates the profound impact of array sparsity on channel decorrelation. Specifically, as the sparsity factors ( $\zeta_{\text{BS}}, \zeta_{\text{IRS}}$ ) increase, the value of  $g_{jk}$  is substantially reduced, indicating that the user channels become increasingly orthogonal. This behavior is attributed to the larger effective apertures, which accentuate the near-field wavefront curvature and thus generate more distinct phase variations across the IRS elements—a phenomenon accurately captured by the  $\Delta_{s,t}$  term in our model. In contrast,

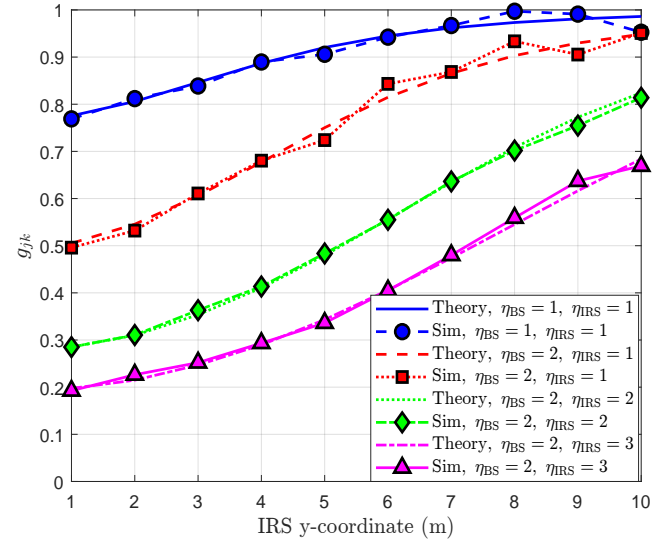


Fig. 4.  $g_{jk}$  versus sparsity and IRS position.

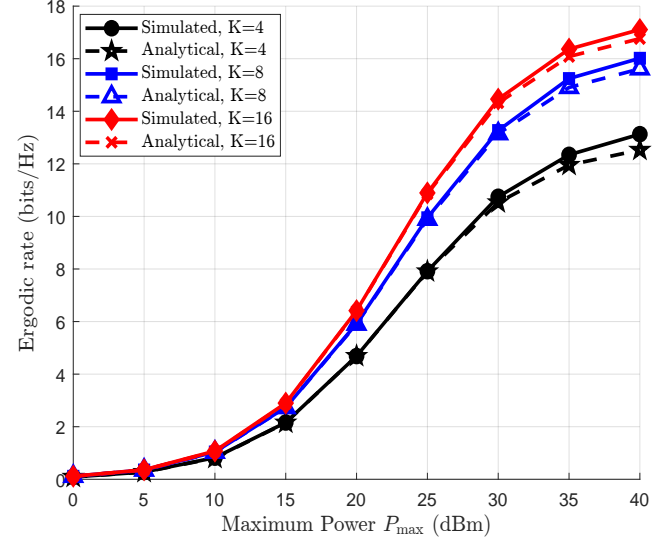


Fig. 5. Ergodic sum-rate versus maximum transmit power  $P_{\text{max}}$  when  $N=400$ .

the conventional dense array setup ( $\zeta_{\text{BS}} = 1, \zeta_{\text{IRS}} = 1$ ) yields a persistently high correlation ( $g_{jk} > 0.75$ ), highlighting the necessity of sparse arrays for achieving favorable propagation in the near-field.

Fig. 5 plots the ergodic sum-rate versus the maximum transmit power  $P_{\text{max}}$  to validate the accuracy of our statistical CSI-based approximation used in problem (42). The analytical results are benchmarked against extensive Monte Carlo simulations for systems with  $K = 4, 8$ , and  $16$  users. An excellent agreement is evident between the analytical and simulated curves for all user loads across the entire power range. This confirms that our approximation, which relies on first and second-order channel statistics, accurately captures the system's long-term performance. Furthermore, the results exhibit the expected monotonic increase in sum-rate with both  $P_{\text{max}}$  and the number of users, which aligns with fundamental system behaviors. The validated accuracy of

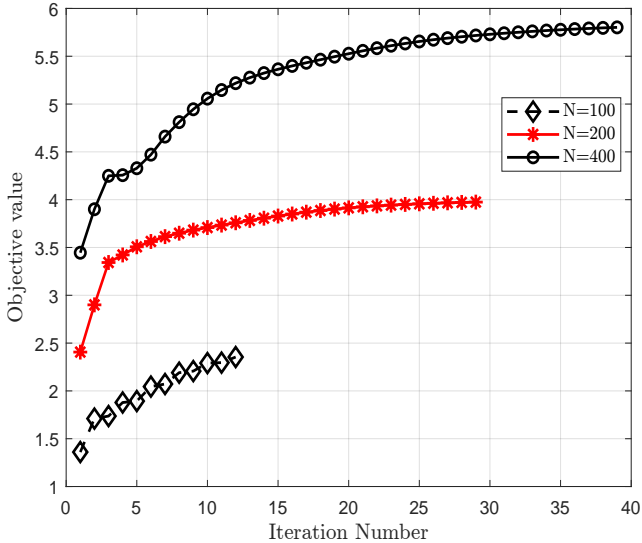
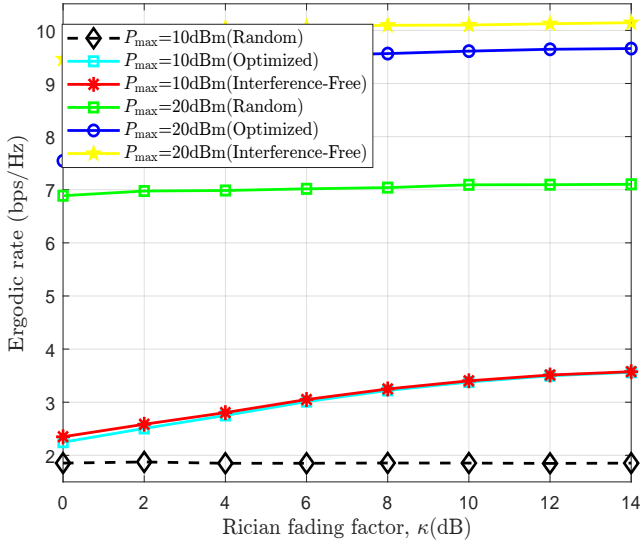


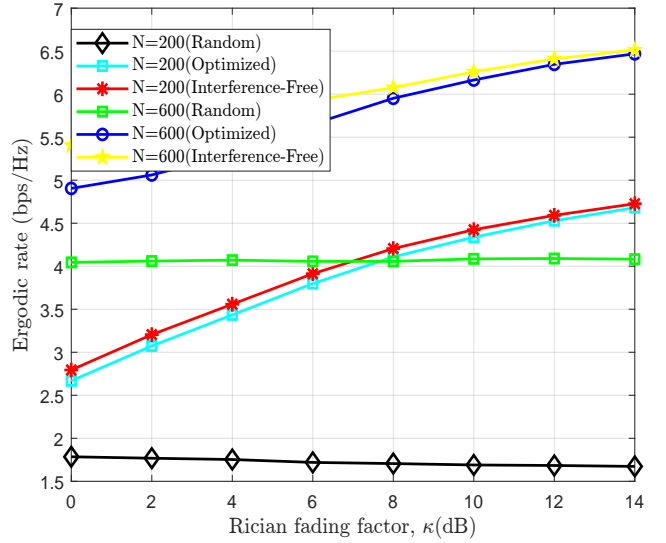
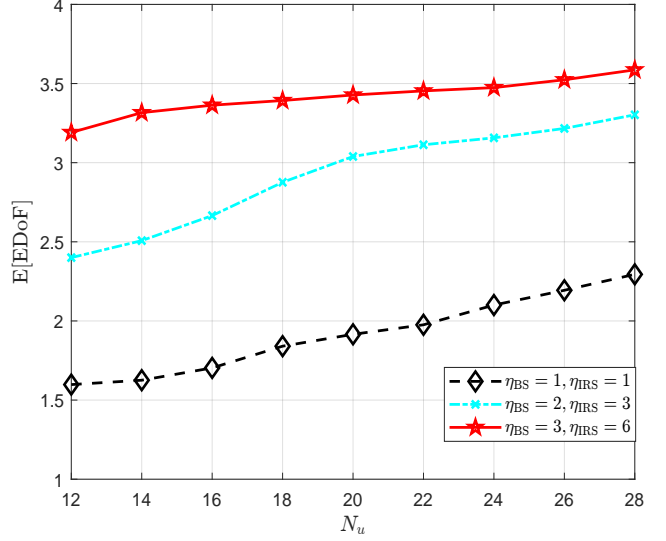
Fig. 6. Convergence behavior of the proposed algorithm.

Fig. 7. Ergodic sum-rate versus Rician factor  $\kappa$  under different transmit power when  $N=600$ .

this approximation justifies its use as a tractable yet reliable objective for the joint optimization of IRS phase shifts and power allocation.

Then, we validate the proposed algorithm's convergence. Fig. 6 shows that the approximate ergodic sum-rate increases monotonically and converges for different numbers of IRS elements  $N$ . This confirms the reliable convergence of our approach. As expected, the results also demonstrate that a larger  $N$  yields substantial performance gains.

Fig. 7 and Fig. 8 investigate the impact of the Rician factor  $\kappa$  on the ergodic sum-rate performance of the proposed algorithm. We benchmark the performance against two schemes, namely (i) Random, in which the IRS phase shifts are randomly selected, and (ii) Interference-Free, a theoretical benchmark that represents the sum-rate achieved with the optimized IRS phase shifts from our algorithm while the inter-user interference term in the SINR expression is hypothetically

Fig. 8. Ergodic sum-rate versus Rician factor  $\kappa$  for different IRS elements when  $P_{\max}=15\text{dBm}$ .Fig. 9.  $\mathbb{E}[\text{EDoF}]$  versus IRS elements.

nullified. As shown in Fig. 7, the optimized design consistently outperforms the Random baseline at both transmit power levels  $P_{\max} = 10\text{dBm}$  and  $P_{\max} = 20\text{dBm}$  throughout the entire range of  $\kappa$ . The performance of all schemes improves as  $\kappa$  increases since a stronger LoS component renders the channel more deterministic and less susceptible to fading. Fig. 8 compares different IRS sizes. Using a larger surface with  $N = 600$  substantially elevates the sum-rate relative to  $N = 200$  and indicates that intelligent phase-shift design becomes increasingly consequential as the system scales. Across these conditions, the optimized curve operates close to the Interference-Free benchmark, evidencing the effectiveness of the proposed deployment and joint optimization in suppressing inter-user interference and maximizing the ergodic sum-rate.

To further quantify the intrinsic channel decorrelation capability engineered by our deployment strategy, Fig. 9 plots the expected EDoF,  $\mathbb{E}[\text{EDoF}]$ , versus the IRS size ( $N_u = N_v$ ) un-

der  $P_{\max} = 15$  dBm. The expectation is computed via Monte Carlo simulations, where the EDoF is averaged over numerous realizations of random IRS phase shifts. This methodology allows us to assess the fundamental quality of the propagation environment itself, isolating the gains from physical deployment from those of a specific phase shift optimization algorithm. As shown, under our proposed deployment condition, the  $\mathbb{E}[\text{EDoF}]$  steadily increases with  $N_u$  and approaches the theoretical maximum of  $K = 4$ . This result signifies that the proposed sparse deployment fundamentally enables the system to achieve full spatial multiplexing gain by creating four nearly orthogonal sub-channels. In contrast, denser array configurations yield a significantly lower  $\mathbb{E}[\text{EDoF}]$ , reinforcing the conclusion that judicious sparse deployment is the critical factor for maximizing the available degrees of freedom.

## VI. CONCLUSION

In this paper, we investigated an IRS-assisted sparse MIMO system and showed that near-field propagation, when exploited by sparse arrays, can serve as a key enabler for effective multi-user spatial multiplexing. Our analysis revealed that near-field effects can substantially alleviate the user-channel correlation bottleneck inherent in far-field models, and we derived a closed-form favorable propagation metric and a geometry-driven deployment rule to guide system design. Furthermore, we showed that deterministic engineering of the IRS phases shapes the user channels into a well-conditioned form that supports robust interference management. For practical Rician fading channels, we developed an efficient alternating optimization algorithm to maximize the ergodic sum-rate by jointly designing the IRS phase shifts and user power allocation based on statistical CSI. Numerical results validated the analysis and demonstrated substantial performance gains, indicating that near-field sparse array engineering is a promising approach for enhancing the spatial multiplexing capability of IRS-assisted communications.

## APPENDIX A

We derive the variance of the inner product  $Y = \mathbf{h}_j^H \mathbf{h}_k$  for  $j \neq k$ . The variance is defined as  $\text{var}\{Y\} = \mathbb{E}[|Y|^2] - |\mathbb{E}[Y]|^2$ .

The inner product can be expanded as  $Y = \sum_{n_1, n_2} T_{n_1, n_2} e^{-j\phi_{n_1}} e^{j\phi_{n_2}}$ , where  $T_{n_a, n_b} \triangleq [\mathbf{g}_j]_{n_a}^* [\mathbf{F}^H \mathbf{F}]_{n_a, n_b} [\mathbf{g}_k]_{n_b}$ . The second moment  $\mathbb{E}[|Y|^2]$  is given by the four-fold summation:

$$\mathbb{E}[|Y|^2] = \sum_{n_1, n_2, n_3, n_4} T_{n_1, n_2} T_{n_3, n_4}^* \mathbb{E}[e^{j\psi(n_1, n_2, n_3, n_4)}], \quad (62)$$

where the phase argument is  $\psi(n_1, n_2, n_3, n_4) = -\phi_{n_1} + \phi_{n_2} + \phi_{n_3} - \phi_{n_4}$ . Given that the phase shifts  $\{\phi_n\}$  are i.i.d. and drawn from  $\mathcal{U}[0, 2\pi]$ , the expectation of the complex exponential is non-zero (and equals 1) if and only if the indices are paired such that the net coefficient of each independent phase variable in the exponent is zero. This condition admits two surviving scenarios for the index pairings:

- (a)  $n_1 = n_2$  and  $n_3 = n_4$ .
- (b)  $n_1 = n_3$  and  $n_2 = n_4$ .

Using the principle of inclusion-exclusion, the second moment is the sum of contributions from case (a) and case (b), minus the contribution from their intersection (where  $n_1 = n_2 = n_3 = n_4$ ).

The contribution from case (a) corresponds to  $\sum_{n_1, n_3} T_{n_1, n_1} T_{n_3, n_3}^* = |\sum_{n=1}^N T_{n, n}|^2 = |\mathbb{E}[Y]|^2$ . The contribution from case (b) corresponds to  $\sum_{n_1, n_2} T_{n_1, n_2} T_{n_1, n_2}^* = \sum_{n_1, n_2} |T_{n_1, n_2}|^2$ . The intersection is the case  $n_1 = n_2 = n_3 = n_4$ , whose contribution is  $\sum_{n=1}^N |T_{n, n}|^2$ .

Combining these yields the second moment:

$$\begin{aligned} \mathbb{E}[|Y|^2] &= |\mathbb{E}[Y]|^2 + \sum_{n_1, n_2} |T_{n_1, n_2}|^2 - \sum_{n=1}^N |T_{n, n}|^2 \\ &= |\mathbb{E}[Y]|^2 + \sum_{n_1 \neq n_2} |T_{n_1, n_2}|^2. \end{aligned} \quad (63)$$

The variance is then found by subtracting  $|\mathbb{E}[Y]|^2$ :

$$\text{var}\{\mathbf{h}_j^H \mathbf{h}_k\} = \sum_{n_1 \neq n_2} |T_{n_1, n_2}|^2. \quad (64)$$

Substituting the definition of  $T_{n_1, n_2}$  gives the final result:

$$\text{var}\{\mathbf{h}_j^H \mathbf{h}_k\} = \sum_{n_1 \neq n_2} |[\mathbf{g}_j]_{n_1}|^2 |[\mathbf{g}_k]_{n_2}|^2 |[\mathbf{F}^H \mathbf{F}]_{n_1, n_2}|^2. \quad (65)$$

## APPENDIX B

We provide the derivations for the statistical moments used in the ergodic rate analysis. The cascaded channel is decomposed as  $\mathbf{h}_k = \bar{\mathbf{h}}_k + \tilde{\mathbf{h}}_k$ , comprising a deterministic LoS component  $\bar{\mathbf{h}}_k = \sqrt{\alpha_k \beta_k} \mathbf{F} \Theta \bar{\mathbf{g}}_k$  and a zero-mean NLoS component  $\tilde{\mathbf{h}}_k = \sqrt{\alpha_k (1 - \beta_k)} \mathbf{F} \Theta \tilde{\mathbf{g}}_k$ , where  $\mathbb{E}[\tilde{\mathbf{g}}_k \tilde{\mathbf{g}}_k^H] = \mathbf{I}_N$ . To facilitate the derivation with respect to the IRS phase shifts  $\boldsymbol{\theta} = [e^{j\phi_1}, \dots, e^{j\phi_N}]^T$ , we utilize the algebraic identity  $\boldsymbol{\Theta} \mathbf{v} = \text{diag}(\mathbf{v}) \boldsymbol{\theta}$  for any vector  $\mathbf{v}$ .

The first moment  $\mathbb{E}[\mathbf{h}_k^H \mathbf{h}_k]$  represents the average channel power. Leveraging the linearity of expectation and the fact that cross-terms vanish due to  $\mathbb{E}[\tilde{\mathbf{h}}_k] = \mathbf{0}$ , we have

$$\begin{aligned} \mathbb{E}[\mathbf{h}_k^H \mathbf{h}_k] &= \|\bar{\mathbf{h}}_k\|^2 + \mathbb{E}[\|\tilde{\mathbf{h}}_k\|^2] \\ &= \alpha_k \beta_k \|\mathbf{F} \text{diag}(\bar{\mathbf{g}}_k) \boldsymbol{\theta}\|^2 + \alpha_k (1 - \beta_k) \text{tr}(\mathbf{F} \boldsymbol{\Theta} \boldsymbol{\Theta}^H \mathbf{F}^H) \\ &= \alpha_k \beta_k \boldsymbol{\theta}^H \mathbf{A}_{k, k} \boldsymbol{\theta} + C_k, \end{aligned} \quad (66)$$

where  $\mathbf{A}_{k, k} \triangleq \text{diag}(\bar{\mathbf{g}}_k)^H \mathbf{F}^H \mathbf{F} \text{diag}(\bar{\mathbf{g}}_k)$  and  $C_k \triangleq \alpha_k (1 - \beta_k) \|\mathbf{F}\|_F^2$ .

Next, we evaluate the second moment  $\mathbb{E}[|\mathbf{h}_k^H \mathbf{h}_j|^2]$  for  $j \neq k$ . Since  $\bar{\mathbf{h}}_k$  and  $\tilde{\mathbf{h}}_j$  are independent zero-mean complex Gaussian vectors, terms involving an odd number of stochastic components evaluate to zero. Consequently, only four terms persist in the expectation:

$$\begin{aligned} \mathbb{E}[|\mathbf{h}_k^H \mathbf{h}_j|^2] &= |\bar{\mathbf{h}}_k^H \bar{\mathbf{h}}_j|^2 + \mathbb{E}[|\bar{\mathbf{h}}_k^H \tilde{\mathbf{h}}_j|^2] \\ &\quad + \mathbb{E}[|\tilde{\mathbf{h}}_k^H \bar{\mathbf{h}}_j|^2] + \mathbb{E}[|\tilde{\mathbf{h}}_k^H \tilde{\mathbf{h}}_j|^2]. \end{aligned} \quad (67)$$

The first term is purely deterministic and can be rewritten as:

$$\begin{aligned} |\bar{\mathbf{h}}_k^H \bar{\mathbf{h}}_j|^2 &= \alpha_k \alpha_j \beta_k \beta_j |\boldsymbol{\theta}^H \text{diag}(\bar{\mathbf{g}}_k)^H \mathbf{F}^H \mathbf{F} \text{diag}(\bar{\mathbf{g}}_j) \boldsymbol{\theta}|^2 \\ &= \alpha_k \alpha_j \beta_k \beta_j |\boldsymbol{\theta}^H \mathbf{A}_{k, j} \boldsymbol{\theta}|^2. \end{aligned} \quad (68)$$

For the cross-terms, we apply the property  $\mathbb{E}[|\mathbf{a}^H \mathbf{z}|^2] = \mathbf{a}^H \mathbb{E}[\mathbf{z} \mathbf{z}^H] \mathbf{a}$ . Substituting the covariance  $\mathbb{E}[\tilde{\mathbf{h}}_j \tilde{\mathbf{h}}_j^H] = \alpha_j(1 - \beta_j)\mathbf{F}\mathbf{F}^H$ , we obtain:

$$\mathbb{E}[|\tilde{\mathbf{h}}_k^H \tilde{\mathbf{h}}_j|^2] = \tilde{\mathbf{h}}_k^H \mathbb{E}[\tilde{\mathbf{h}}_j \tilde{\mathbf{h}}_j^H] \tilde{\mathbf{h}}_k = \alpha_k \alpha_j \beta_k (1 - \beta_j) \mathbf{\theta}^H \mathbf{D}_k \mathbf{\theta}, \quad (69)$$

where  $\mathbf{D}_k \triangleq \text{diag}(\bar{\mathbf{g}}_k)^H \mathbf{F}^H (\mathbf{F} \mathbf{F}^H) \mathbf{F} \text{diag}(\bar{\mathbf{g}}_k)$ . By symmetry, the third term is  $\mathbb{E}[|\tilde{\mathbf{h}}_k^H \tilde{\mathbf{h}}_j|^2] = \alpha_k \alpha_j \beta_j (1 - \beta_k) \mathbf{\theta}^H \mathbf{D}_j \mathbf{\theta}$ .

The final NLoS-NLoS interaction term involves the fourth-order moment. Using the standard property  $\mathbb{E}[|\mathbf{x}^H \mathbf{y}|^2] = \text{tr}(\mathbf{x} \mathbf{x}^H \mathbf{y} \mathbf{y}^H)$  for independent Gaussian vectors, we derive:

$$\begin{aligned} \mathbb{E}[|\tilde{\mathbf{h}}_k^H \tilde{\mathbf{h}}_j|^2] &= \text{tr}(\alpha_k(1 - \beta_k)\mathbf{F}\mathbf{F}^H \cdot \alpha_j(1 - \beta_j)\mathbf{F}\mathbf{F}^H) \\ &= \alpha_k \alpha_j (1 - \beta_k)(1 - \beta_j) \text{tr}((\mathbf{F}\mathbf{F}^H)^2). \end{aligned} \quad (70)$$

Summing these components yields the expressions in (39) and (40).

## REFERENCES

- [1] C.-X. Wang, X. You, X. Gao, X. Zhu, Z. Li, C. Zhang, H. Wang, Y. Huang, Y. Chen, H. Haas, J. S. Thompson, E. G. Larsson, M. D. Renzo, W. Tong, P. Zhu, X. Shen, H. V. Poor, and L. Hanzo, "On the road to 6G: Visions, requirements, key technologies, and testbeds," *IEEE Commun. Surveys Tuts.*, vol. 25, no. 2, pp. 905–974, Feb. 2023.
- [2] Z. Wang, J. Zhang, H. Du, D. Niyato, S. Cui, B. Ai, M. Debbah, K. B. Letaief, and H. V. Poor, "A tutorial on extremely large-scale MIMO for 6G: Fundamentals, signal processing, and applications," *IEEE Commun. Surveys Tuts.*, vol. 26, no. 3, pp. 1560–1605, Jan. 2024.
- [3] M. Cui, Z. Wu, Y. Lu, X. Wei, and L. Dai, "Near-field mimo communications for 6G: Fundamentals, challenges, potentials, and future directions," *IEEE Commun. Mag.*, vol. 61, no. 1, pp. 40–46, Sep. 2023.
- [4] H. Zhang, N. Shlezinger, F. Guidi, D. Dardari, and Y. C. Eldar, "6G wireless communications: From far-field beam steering to near-field beam focusing," *IEEE Commun. Mag.*, vol. 61, no. 4, pp. 72–77, Mar. 2023.
- [5] X. Li, Z. Dong, Y. Zeng, S. Jin, and R. Zhang, "Multi-user modular xl-mimo communications: Near-field beam focusing pattern and user grouping," *IEEE Trans. Wireless Commun.*, vol. 23, no. 10, pp. 13 766–13 781, May 2024.
- [6] H. Lu, Y. Zeng, C. You, Y. Han, J. Zhang, Z. Wang, Z. Dong, S. Jin, C.-X. Wang, T. Jiang, X. You, and R. Zhang, "A tutorial on near-field XL-MIMO communications toward 6G," *IEEE Commun. Surveys Tuts.*, vol. 26, no. 4, pp. 2213–2257, Apr. 2024.
- [7] X. Chen, H. Ren, C. Pan, Z. Peng, and J. Wang, "Effective dof-oriented optimal antenna spacing in near-field XL-MIMO systems," *arXiv preprint arXiv:2501.07062*, 2025.
- [8] H. Lu and Y. Zeng, "Near-field modeling and performance analysis for multi-user extremely large-scale MIMO communication," *IEEE Communications Letters*, vol. 26, no. 2, pp. 277–281, Nov. 2022.
- [9] Y. Liu, J. Xu, Z. Wang, X. Mu, and L. Hanzo, "Near-field communications: What will be different?" *IEEE Wireless Communications*, vol. 32, no. 2, pp. 262–270, Mar. 2025.
- [10] H. Wang, C. Feng, Y. Zeng, S. Jin, C. Yuen, B. Clerckx, and R. Zhang, "Enhancing spatial multiplexing and interference suppression for near- and far-field communications with sparse MIMO," *arXiv preprint arXiv:2408.01956*, 2024.
- [11] Y. Zhuang, X. Zhang, Z. He, M. S. Greco, and F. Gini, "Sparse array design via integer linear programming," *IEEE Trans. Signal Process.*, vol. 72, pp. 4812–4826, Sep. 2024.
- [12] X. Li, H. Min, Y. Zeng, S. Jin, L. Dai, Y. Yuan, and R. Zhang, "Sparse mimo for isac: New opportunities and challenges," *IEEE Wireless Commun.*, vol. 32, no. 4, pp. 170–178, Mar. 2025.
- [13] C. Zhou, C. You, H. Zhang, L. Chen, and S. Shi, "Sparse array enabled near-field communications: Beam pattern analysis and hybrid beamforming design," *arXiv preprint arXiv:2401.05690*, 2024.
- [14] K. Chen, C. Qi, G. Y. Li, and O. A. Dobre, "Near-field multiuser communications based on sparse arrays," *IEEE J. Sel. Topics Signal Process.*, vol. 18, no. 4, pp. 619–632, Jun. 2024.
- [15] K. Chen, C. Qi, J. Huang, O. A. Dobre, and G. Y. Li, "Near-field communications for extremely large-scale MIMO: A beamspace perspective," *IEEE Commun. Mag.*, vol. 63, no. 5, pp. 166–172, Jan. 2025.
- [16] D. Dardari, "Communicating with large intelligent surfaces: Fundamental limits and models," *IEEE J. Sel. Areas Commun.*, vol. 38, no. 11, pp. 2526–2537, Jul. 2020.
- [17] Q. Tao, S. Zhang, C. Zhong, W. Xu, H. Lin, and Z. Zhang, "Weighted sum-rate of intelligent reflecting surface aided multiuser downlink transmission with statistical csi," *IEEE Trans. Wireless Commun.*, vol. 21, no. 7, pp. 4925–4937, Jul. 2022.
- [18] Q. Wu, Y. Zhu, Q. Peng, W. Hao, Y. Hou, F. Yang, W. Yan, G. Wang, W. Chen, and C. Qiu, "Intelligent reflecting surfaces for THz communications: Fundamentals, key solutions, and system prototyping," *arXiv preprint arXiv:2506.17200*, 2025.
- [19] X. Mo, L. Gui, K. Ying, X. Sang, and X. Diao, "Reconfigurable intelligent surface deployment for wideband millimeter wave systems," *IEEE Trans. Commun.*, vol. 72, no. 5, pp. 2989–3004, Jan. 2024.
- [20] Y. Cheng, W. Peng, C. Huang, G. C. Alexandropoulos, C. Yuen, and M. Debbah, "RIS-aided wireless communications: Extra degrees of freedom via rotation and location optimization," *IEEE Trans. Wireless Commun.*, vol. 21, no. 8, pp. 6656–6671, Mar. 2022.
- [21] J. Bai, Q. Yan, H.-M. Wang, and Y. Liu, "Intelligent reflecting surface aided green communication with deployment optimization," *IEEE Trans. Commun.*, vol. 72, no. 8, pp. 5130–5144, Mar. 2024.
- [22] C. Huang, A. Zappone, G. C. Alexandropoulos, M. Debbah, and C. Yuen, "Reconfigurable intelligent surfaces for energy efficiency in wireless communication," *IEEE Trans. Wireless Commun.*, vol. 18, no. 8, pp. 4157–4170, Jun. 2019.
- [23] I. Santamaria, M. Soleimani, E. Jorswieck, and J. Gutiérrez, "Interference leakage minimization in RIS-assisted MIMO interference channels," in *Proc. IEEE Int. Conf. Acoust., Speech Signal Process. (ICASSP)*, Jun. 2023, pp. 1–5.
- [24] W. Liu, A. Li, Y. Xu, Z. Zhang, Y. Zhang, and B. Jiang, "RIS-aided interference subspace alignment for k -user MIMO interference networks," *IEEE Commun. Lett.*, vol. 28, no. 8, pp. 1919–1923, Jun. 2024.
- [25] X. Gan, C. Zhong, C. Huang, and Z. Zhang, "RIS-assisted multi-user MISO communications exploiting statistical csi," *IEEE Trans. Commun.*, vol. 69, no. 10, pp. 6781–6792, Jul. 2021.
- [26] K. Zhi, C. Pan, H. Ren, and K. Wang, "Power scaling law analysis and phase shift optimization of RIS-aided massive mimo systems with statistical csi," *IEEE Trans. Commun.*, vol. 70, no. 5, pp. 3558–3574, Mar. 2022.
- [27] Q. Wu, G. Chen, Q. Peng, W. Chen, Y. Yuan, Z. Cheng, J. Dou, Z. Zhao, and P. Li, "Intelligent reflecting surfaces for wireless networks: Deployment architectures, key solutions, and field trials," *IEEE Wireless Commun.*, pp. 1–9, May 2025.
- [28] Y. Chen, Q. Wu, G. Chen, and W. Chen, "Spatial multiplexing oriented channel reconfiguration in multi-IRS aided MIMO systems," *IEEE Trans. Veh. Technol.*, vol. 74, no. 6, pp. 9840–9845, Feb. 2025.
- [29] W. Chen, C.-K. Wen, X. Li, and S. Jin, "Channel customization for joint Tx-RISs-Rx design in hybrid mmWave systems," *IEEE Trans. Wireless Commun.*, vol. 22, no. 11, pp. 8304–8319, Nov. 2023.
- [30] X. Cui, K.-H. Park, and M.-S. Alouini, "Channel capacity saturation point and beamforming acceleration for near-field XL-MIMO multiuser communications," *arXiv preprint arXiv:2503.18118*, 2025.
- [31] Z. Wang, J. Zhang, W. Yi, H. Xiao, H. Du, D. Niyato, B. Ai, and D. W. K. Ng, "Analytical framework for effective degrees of freedom in near-field XL-MIMO," *IEEE Trans. Wireless Commun.*, vol. 24, no. 4, pp. 3465–3482, Jan. 2025.
- [32] Z. Wang, J. Zhang, H. Du, W. E. I. Sha, B. Ai, D. Niyato, and M. Debbah, "Extremely large-scale MIMO: Fundamentals, challenges, solutions, and future directions," *IEEE Wireless Commun.*, vol. 31, no. 3, pp. 117–124, Apr. 2024.
- [33] M. Cui and L. Dai, "Near-field wideband beamforming for extremely large antenna arrays," *IEEE Trans. Commun.*, vol. 23, no. 10, pp. 13 110–13 124, Oct. 2024.
- [34] S. Sun, R. Li, C. Han, X. Liu, L. Xue, and M. Tao, "How to differentiate between near field and far field: Revisiting the rayleigh distance," *IEEE Commun. Mag.*, vol. 63, no. 1, pp. 22–28, Jan. 2025.
- [35] G. Interdonato, F. Di Murro, C. D'Andrea, G. Di Gennaro, and S. Buzzi, "Approaching massive MIMO performance with reconfigurable intelligent surfaces: We do not need many antennas," *IEEE Trans. Commun.*, vol. 73, no. 6, pp. 4000–4016, Nov. 2024.
- [36] Z. Kang, C. You, and R. Zhang, "Active-passive IRS aided wireless communication: New hybrid architecture and elements allocation optimization," *IEEE Trans. Wireless Commun.*, vol. 23, no. 4, pp. 3450–3464, Apr. 2024.

- [37] K. Shen and W. Yu, "Fractional programming for communication systems—part i: Power control and beamforming," *IEEE Trans. Signal Process.*, vol. 66, no. 10, pp. 2616–2630, May 2018.
- [38] K. Shen and W. Yu, "Fractional programming for communication systems—part ii: Uplink scheduling via matching," *IEEE Trans. Signal Process.*, vol. 66, no. 10, pp. 2631–2644, May 2018.
- [39] M. Grant, "Cvx: Matlab software for disciplined convex programming, version 1.21," <http://cvxr.com/cvx>, 2011.